HHS Public Access

Author manuscript

Magn Reson Med. Author manuscript; available in PMC 2016 December 01.

Published in final edited form as:

Magn Reson Med. 2015 December ; 74(6): 1609–1620. doi:10.1002/mrm.25560.

Contrast Enhancement by Combining T1- and T2-weighted Structural Brain MR Images

Masaya Misaki[1], **Jonathan Savitz**[1,2], **Vadim Zotev**[1], **Raquel Phillips**[1], **Han Yuan**[1], **Kymberly D. Young**[1], **Wayne C. Drevets**[1,3], and **Jerzy Bodurka**[1,4,#]

[1]Laureate Institute for Brain Research, Tulsa, OK, United States

[2]Faculty of Community Medicine, University of Tulsa, Tulsa, OK, United States

[3]Janssen Pharmaceuticals, LCC, of Johnson & Johnson, Inc., Titusville, NJ, USA

[4]College of Engineering, University of Oklahoma, Tulsa, OK, United States

Abstract

Purpose—In order to more precisely differentiate cerebral structures in neuroimaging studies, a novel technique for enhancing the tissue contrast based on a combination of T1-weighetd (T1w) and T2-weighed (T2w) magnetic resonance imaging (MRI) images was developed.

Methods—The combined image (CI) was calculated as CI = (T1w−**s**T2w)/(T1w+sT2w), where sT2w is the scaled T2-weighted image. The scaling factor was calculated to adjust the gray matter voxel intensities in the T2w image so that their median value equaled that of the gray matter voxel intensities in the T1w image. The image intensity homogeneity within a tissue and the discriminability between tissues in the CI versus the separate T1w and T2w images were evaluated using the segmentation by FSL and FreeSurfer software.

Results—The combined image significantly improved homogeneity in the white and gray matter compared to the T1w images alone. The discriminability between white and gray matter also improved significantly by applying the CI approach. Significant enhancements to the homogeneity and discriminability also were achieved in most subcortical nuclei tested, with the exception of the amygdala and the thalamus.

Conclusion—The tissue discriminability enhancement offered by the CI potentially enables more accurate neuromorphometric analyses of brain structures.

Keywords

MRI contrast enhancement; T1- T2-weighted image fusion; tissue segmentation; subcortical segmentation

[#]Corresponding author: Jerzy Bodurka, 6655 South Yale Avenue, Tulsa, OK. 74136. TEL: +1-918-502-5101. jbodurka@laureateinstitute.org.

Introduction

The accuracy and sensitivity of in vivo brain structural analyses based on magnetic resonance imaging (MRI) are critically dependent on the acquisition of structural MR images characterized by both high spatial resolution and high tissue contrast. In MRI-based brain structural analysis, the T1-weighted image (T1w) is the contrast type that is most commonly used to delineate brain structures. While the utility of T1w images has been well established and recent advances in scanning sequences have resulted in T1 contrast improvements (1,2), some of the boundaries of brain structures remain ambiguous in these images. T1 spin-lattice relaxation times of subcortical structures, for example, fall between those of cortical gray matter and white matter (3-5), so that enhancing T1 contrast only might not be sufficient to delineate these structures. The use of other MRI-based image contrasts conceivably may enhance the accuracy of delineating structural boundaries.

The utility of using multiple MRI contrasts via sequential acquisition of images with different weighting has been established in many studies for detecting tissue pathology, such as multiple sclerosis lesions (6-9), tumors (10-12), iron deposition (13), nonspecific signal hyperintensities (14), and regional atrophy (15-17). Also in neuromorphometric analyses, images with different weighting including T1-weighted, T2-weighted (T2w), and proton density (PD) images have been used to segment gray matter, white matter, and cerebrospinal fluid (CSF) regions (18-20). These tissue segmentation analyses search clusters or boundaries in the multivariate space to classify a specific brain tissue and output discrete segmentation maps or probabilistic maps of segmented tissues.

Instead of creating multiple segmented maps, several studies combined images with different weightings to reconstruct a single (or fusion) image with improved quality. Van de Moortele, et al. (21) utilized PD image to improve T1w image in 7T. Helms, et al. (22) and Glasser, et al. (23) used the T2w image to refine the placement of pial surface and exclude non-brain regions on the T1w image. Rilling, et al. (24) used T1w and T2w images to estimate and correct the bias field of the images. Glasser and Van Essen (25) also utilized the T1w and T2w images together to create a single image by dividing the T1w with the T2w. This T1w/T2w ratio combination image can enhance contrast of myelin content.

In line with these image fusion approaches, we propose a novel combination of T1w and T2w images. The combined image (CI) is primarily aimed to improve image quality by enhancing tissue discriminability in the brain. This article describes how to create the CI and how it enhances homogeneity and discriminability of brain tissues in the Theory section. We then evaluated the image quality of the CI compared to T1w in the Methods and Results sections. As a measure of image quality, we evaluated two scales; intensity homogeneity within a tissue and discriminability between tissues in MR image. We used two independent datasets for the evaluation; images scanned at our site (Laureate Institute for Brain Research, LIBR) and images from the Human Connectome Project (HCP) (26). By comparing the results from different MRI vendors, different sites and different scanning parameters, we confirm that the discriminability enhancement of the CI is applicable to general T1w and T2w MRI images.

Theory

The CI is calculated as (T1w−sT2w)/(T1w+sT2w), where sT2w is a scaled T2w image. The scaling value was calculated such that the median value of gray matter voxels in the T2w image equaled the median value of gray matter voxels in the T1w image. The detailed procedure of creating CI is described in the Method section. In this section, theoretical concept of CI is described.

The CI calculation is composed of three parts; scaling the T2w image, subtracting the scaled T2w image from the T1w image, and normalizing the subtracted values by the sum of the T1w image and the scaled T2w image.

The subtraction procedure provides the main component of image contrast. This contrast takes advantage of the fact that the contrast directions of T1w and T2w images are opposite across brain tissues. Namely, the T2w image has high signal in cerebrospinal fluid (CSF), low signal in white matter (WM), and an intermediate value in gray matter (GM), whereas the T1w image has low CSF signal, high WM signal, and intermediate value GM signal. We therefore hypothesized that the subtraction of the T2w image from the T1w image could enhance the tissue contrast due to the complementary signal properties of CSF and WM in the context of similar signal intensities in GM.

The purpose of scaling the T2w image is to compensate for the arbitrariness of value units in MR images. T1w and T2w images do not indicate the absolute value of T1 and T2 relaxation times but rather the image values depend on scanning parameters and tissues properties (27). We therefore scaled the images in order to make the CI immune to such variability. Since the CI attempts to utilize the opposite contrast direction across WM, GM, and CSF, the image value is adjusted according to the signal intensity in the gray matter region such that the median value of gray matter voxels in the T2w image equals the median value of gray matter voxels in the T1w image.

Lastly, the normalization factor (dividing by T1w+sT2w) cancels out the inhomogeneity of image intensities. This scaling normalizes image values to the same range in all voxels regardless of absolute intensity size: from −1.0 to 1.0 with negative values in the CSF, positive values in the WM, and values near 0 in the GM. This normalization makes the CI sensitive only to the relative difference of T1w and sT2w in a voxel and removes any variability in the sum of T1w and sT2w values across voxels. While this only helps to remove B1- inhomogeneity, it is still the dominating inhomogeneity at 3T using a multi-channel receive-only array coil.

Figure 1 demonstrates how the CI enhances tissue discriminability by combining T1w and T2w images for a representative subject from the LIBR sample. The two columns on the reader's left show one coronal slice of T1w, T2w, T1w-sT2w, and CI images and their zoomed regions. The column on the reader's right shows the distributions of the image values within WM and GM voxels. Note that the direction of the horizontal axis of T2w plot was reversed for the comparisons of the other image types. WM and GM brain tissue segmentation was performed with FAST from FSL as described in the Methods section.

The GM and WM voxel value distributions indicated that the difference of the mean values between the GM and the WM in the T1w image was large, but the variance of the WM was also large, resulting in overlap in the range of values between the GM and WM. The T2w image had a skewed distribution for both GM and WM with long tails indicating lower homogeneity and discriminability for these tissues. The T1w-sT2w image showed lower variability within WM as well as a large difference between WM and GM. Scaling by the T1w+sT2w reduced the variance of WM still further. As a result, CI reduced the overlap of intensity values between WM and GM and provided better discriminability between tissues.

This image contrast enhancement was demonstrated not only for this slice of this subject. Supporting figure S1 shows images of multiple slices for this subject and supporting figure S2 shows sample slices for another four representative subjects in the LIBR dataset.

Methods

In order to quantify the quality enhancement provided by the CI, we evaluated the tissue homogeneity and discriminability of the CI compared to the T1w and T2w images. Here we used two datasets; images scanned at our site (LIBR) and images from the Human Connectome Project (HCP) (26).

LIBR data

Twenty three healthy volunteers (age 20–53 years, mean±SD = 34±10 years, 12 female) participated in the study. Imaging was conducted on a whole-body 3 tesla MRI scanner (Discovery MR750, GE Healthcare, Milwaukee, WI) equipped with a 32ch receive-only head array coil (Nova Medical). The structural image scan was performed as a part of other functional studies (28,29). The studies were approved by the institutional review board of the University of Oklahoma and the Western Institutional Review Board. All subjects gave written informed consent to participate in the study and received financial compensation.

The T1w images were obtained with the magnetization-prepared rapid gradient-echo (MPRAGE) sequence with the following parameters: TR = 9 ms, TE = 3.372 ms, TI = 725 ms, TD = 1400ms, flip angle = 8°, sensitivity encoding (SENSE) acceleration factor R = 2, FOV = 240 mm × 192 mm, 80 coronal slices, slice thickness = 2.0 mm, voxel size = 0.47 × 0.47 × 2.00 mm^3, scan time = 10 min 4 s. The image was centered on the basal ganglia and midbrain region. The T1w image with the same parameters was obtained twice for nine of the subjects (age 20-45 years, mean±SD = 29±9 years, 5 female) to evaluate the effect of averaging T1w images on the image quality in comparison with the CI.

The T2w images were obtained with the Fast Spin Echo PROPELLER sequence with the following parameters: TR = 10.124–13.704 s, TE = 124–150 ms (TR and TE differed across subjects), flip angle = 90.00 or 142.35°, FOV = 240 × 240 mm, 80 coronal slices, slice thickness = 2.0 mm, voxel size = 0.47 × 0.47 × 2.00 mm^3, scan time = 7 min 26 s–14 m 60 s. The TR and TE were adjusted for each subject due to the specific absorption rate (SAR) limit. The T2w image covered the same regional volume as the T1w image. T1w and T2w images were acquired in consecutive scans with the same head position in the scanner. The T2w image was aligned to the T1w image using *align_epi_anat.py* script in AFNI (30).

In addition to these coronal-plane high-resolution, partial-coverage images, standard-resolution T1-weighted images covering the whole brain also were obtained for registering the individual brain images to the template space, which was necessary for the segmentation analyses using FSL-FAST (http://fsl.fmrib.ox.ac.uk/fsl/fslwiki/FAST) and FreeSurfer (https://surfer.nmr.mgh.harvard.edu) software in the image quality evaluation. Scanning parameters for this whole-brain structural MRI image were TR = 5 ms, TE = 2 ms, TI = 725 ms, flip angle = 8°, SENSE acceleration factor R = 2, FOV = 240 × 192 mm, 186 axial slices, slice thickness = 0.9 mm, voxel size = 0.94 × 0.94 × 0.90 mm^3, scan time = 5 min 40 s.

HCP data

We used the HCP structural preprocessed data of 38 unrelated subjects in the release Q3 (23). The data included 21 female and their ages were from 22 to 35 except one female over 35 (HCP does not disclose exact age of the subjects). Since scanning parameters of HCP data are described in Glasser, et al. (23), only a summary of them are reproduced here.

The images were acquired on the HCP's custom 3 T Siemens Skyra MRI scanner (31) with a 32-channel head coil. The T1w image was 3D MPRAGE images with 0.7 mm isotropic resolution, FOV = 224 mm, matrix = 320, 256 sagittal slices in a single slab, TR = 2400 ms, TE = 2.14 ms, TI = 1000 ms, FA = 8°, GRAPPA = 2. The T2w image was the variable flip angle turbo spin-echo sequence with 0.7 mm isotropic resolution (same matrix, FOV, and slices as in the T1w), TR = 3200 ms, TE = 565 ms, GRAPPA = 2. The T1w and T2w images were acquired twice and the average of two separate scans was used only if both scans were not blurry.

We used the preprocessed images (T1w_acpc_dc_restore_brain.nii.gz, T2w_acpc_dc_restore_brain.nii.gz) for our analysis. The preprocessed images were applied gradient distortion correction, ACPC registration, brain extraction, registration of the T2w image to the T1w image, field map distortion correction, and bias field correction using sqrt(T1w × T2w) (24). The preprocessing procedures are described in Glasser, et al. (23) and WU-Minn HCP Quarter 3 Data Release Reference Manual (http://humanconnectome.org/documentation/Q3/Q3_Release_Reference_Manual.pdf) in more detail.

Creating the combined image

The identical image processing procedures were applied to both the LIBR and the HCP data except where noted. The scaling value for the T2w was calculated to adjust the gray matter voxel intensities in the T2w image so that their median value equaled that of the gray matter voxel intensities in the T1w image. Gray matter voxels were extracted using information from a probabilistic atlas, namely the ICBM 2009c Nonlinear Asymmetric template (http://www.bic.mni.mcgill.ca/ServicesAtlases/ICBM152NLin2009) (32). The template brain T1w image was warped to an individual T1w image using the Advanced Normalization Tools (ANTS; http://www.picsl.upenn.edu/ANTS/) (33). Tissue probability maps for the template brain also were warped to the individual brains using the same warping parameters. Subsequently, gray matter voxels were extracted from the warped tissue probability map as the gray matter probability was larger than 0.5. The scaling factor was calculated as

M_{G_T1}/M_{G_T2}, where M_{G_T1} and M_{G_T2} are the median values of gray matter voxels of T1w and T2w respectively. The term "sT2w" designates the T2w image scaled by this value: $sT2w = M_{G\_T1}/M_{G\_T2} \times T2w$.

For both T1w and sT2w, a region mask was generated using *3dAutomask* program in AFNI. The combined image was created within the union of these masks. 3dAutomask removes the regions with very small intensity value, so that the union mask indicates the region where either T1w or sT2w image has signal value excluding background region.

The T1w and sT2w were combined using the equation $CI = (T1w-sT2w)/(T1w+sT2w)$, as implemented using *3dcalc* in AFNI. The CI image values range from −1.0 to 1.0 with negative values in the CSF, positive values in the white matter, and values near 0 in the gray matter. To facilitate visualization and image processing, the CI was scaled within the union mask to set the minimum at zero and the median at a value where the median intensity of all voxels equaled that of the T1w image.

We generated an average of two T1w images for nine of the subjects in the LIBR data to compare its quality to that of the CI. The intensity inhomogeneity correction was applied to the two T1w images using *N4BiasFieldCorrection* (34) in ANTS. The corrected images were aligned using *mri_robust_register* in FreeSurfer and averaged using *3dcalc* in AFNI. We refer this image as "T1wx2". We also generated a T1w/T2w image to compare its homogeneity and discriminability with the CI. For the HCP data, provided preprocessed files of T1w/T2w (T1wDividedByT2w.nii.gz) were used. Note that the T1w/T2w and CI combinations have different purposes (Fig. 1), regardless of similarity of the fusion equations. The comparison between the CI and T1w/T2w, therefore, was done not for judging which one is better but for showing the difference.

Image quality evaluation

We evaluated homogeneity of image intensity within a tissue and discriminability between tissues as measures of image quality. The homogeneity was calculated as a quotient of the mean value by the standard deviation. The discriminability was calculated by the Fisher score (FS), which indicates how large the difference of mean image intensities between classes relative to the squared sum of variances in each class; $FS = (\mu_{WM}-\mu_{GM})/\mathrm{sqrt}(\sigma_{WM}^2+\sigma_{GM}^2)$ (35), where, μ_{WM}, μ_{GM} and σ_{WM}, σ_{GM} are the means and the standard deviations of white and gray matter voxels, respectively.

To evaluate the homogeneity and the discriminability of white and gray matter regions, we used the tissue segmentation by FAST from FSL (http://fsl.fmrib.ox.ac.uk/fsl/fslwiki/FAST) to obtain tissue segmentation maps. *A-priori* tissue probability maps were used to initialize the segmentation ('-a' option was used in the command line).

For the LIBR data we used the whole-brain T1-weighed image for this *a priori* initialization and for creating a brain mask. The whole-brain image was aligned to the partial-coverage image and then the alignment of the template brain to that of an individual brain was estimated using the *flirt* in FSL. The brain mask was extracted by the *bet* command in FSL and applied to the images before the segmentation.

The FAST segmentation map was used for evaluating the homogeneity of white and gray matter and the discriminability (FS) between them. Since the T2w and T1w/T2w images could not be segmented properly in several subjects, the segmentation map from the T1w image was used for the homogeneity and the discriminability evaluations.

The homogeneity and discriminability across subcortical structures were also evaluated using the segmentation algorithms within FreeSurfer (https://surfer.nmr.mgh.harvard.edu). Since the default processing stream of FreeSurfer could not process a partial coverage image while maintaining high spatial resolution, we developed a custom processing stream. The detailed procedure is described in the supporting material. In this custom procedure, the images were resampled to $0.469mm^3$ isotropic voxels for the LIBR data and kept to $0.7mm^3$ isotropic voxels for the HCP data. The subcortical segmentation map (aseg.mgz) generated by FreeSurfer was used to extract the subcortical regions. Since FreeSurfer could not process T2w and T1w/T2w images, the segmentation map from the T1w image was used for the homogeneity and discriminability evaluation for these images. Seven subcortical structures: thalamus-proper, caudate, putamen, pallidum, hippocampus, amygdala, and accumbens-area were extracted for this evaluation, since only these regions were segmented in all subjects. The discriminability of subcortical structures was evaluated with an average FS between a region and all adjacent segmented structures.

For the LIBR data, homogeneity of the T1w and the T2w images could be significantly reduced due to remaining image inhomogeneity (bias field). To eliminate this effect in the comparison of image quality, intensity inhomogeneity correction with *N4BiasFieldCorrection* in ANTS (34) was applied to the T1w and T2w images in the LIBR data before evaluating the homogeneity and FS values. This correction fitted Gaussian models of multiple resolutions to evaluate the low-frequency intensity inhomogeneity profile and remove the estimated profile from the image. We note that this correction was applied only for evaluating quality of T1w and T2w as independent images and no correction was applied to the CI, T1w/T2w, and its source images. Namely, any homogeneity improvement of the CI depends only on the implementation of the CI calculation. Since the LIBR images covered a partial region and the signal intensities at edge slices were diminished, the quality evaluation was restricted to the volume in the image mask created using 3dAutomask for the T1w image in order to exclude the edge slices.

Statistical analyses for the difference of the image quality measures were performed with the Linear Mixed Effect (LME) model analysis (36) on the R statistical computing language and environment (37). Average of the left and right hemispheres of each region was entered as a dependent variable. Image type and sex were entered as fixed effects and subject as a random effect. For the LIBR data, age and T2 scan parameters (TR, TE, and flip angle) were also entered as fixed effects since different T2 scan parameters were used across subjects. For the HCP data, since exact subjects' age was not disclosed and the same scan parameters were used for all the subjects, these variables were not entered in the analysis. For the statistical test for subcortical area, region was also entered as a fixed effect. Multiple comparisons were performed with the Tukey's multiple comparison test. We also employed the nonparametric statistical tests, the Friedman test and the Wilcoxon signed rank test, for the evaluation of T1wx2 image quality since the number of subjects was small for this data.

Results

Homogeneity and discriminability in the white and gray matters

Figure 2a shows the white and gray matter homogeneity and the discriminability of the CI, T1w, T2w, and T1w/T2w in the LIBR data. Table 1a shows the statistics of the LME analysis. The main effect of image type was significant in the homogeneity of white matter, gray matter, and the discriminability (FS) between them. Tukey's multiple comparison test revealed all pairs of image type differences were significant with $P < 0.001$ except between T2w and T1w/T2w ($P = .092$). These results indicate that the CI had significant improvement of tissue homogeneity in both white matter and gray matter as well as discriminability between white matter and gray matter compared to T1w image.

In the LIBR data, CI was compared also to the T1wx2 images for nine of the subjects (Figure 2b). The Wilcoxon signed rank test showed that the difference between the CI and the T1wx2 image was significant in white matter homogeneity ($P = 0.004$), gray matter homogeneity ($P = 0.004$), and the FS between them ($P = 0.004$).

For the HCP data (Figure 2c and Table 1b), the main effect of image type was significant in the homogeneity of white matter, gray matter, and FS between them. Tukey's multiple comparison test indicated all pairs of image type differences were significant with $P < 0.001$ for all measures.

These results indicated that the CI had significant improvement of the tissue homogeneity in white matter and gray matter and the discriminability between them compared to T1w and T2w. The improvement was observed consistently in both LIBR and HCP data. The CI also showed significant improvement even when compared against the average of two T1w images for the LIBR data.

Homogeneity and discriminability in subcortical regions

For the LIBR data (Figure 3 and Table 2a), the main effect of image type was significant for the homogeneity and the discriminability. Tukey's multiple comparison test between the image types indicated that when averaged across regions both the homogeneity and discriminability of the CI were significantly higher than those of the T1w image ($P < 0.001$). A significant effect of the region and the interaction between image type and region were seen in both homogeneity and discriminability. Sex and TE of T2w image had also significant effects on homogeneity (shorter TE and female subjects had higher homogeneity).

Table 3 shows the results of Tukey's multiple comparison test between image types in each region. The CI showed a significant increase in homogeneity for all the regions assessed and a significant increase in discriminability for all the regions assessed except for the amygdala compared to the T1w image. In the comparison to the T2w and T1w/T2w images, the CI showed a significant increase in both homogeneity and discriminability in all the regions.

Figure 4 shows the comparison with the T1wx2 image for nine of the subjects in the LIBR dataset. Table 4 shows the results of the Wilcoxon signed rank test between the image types

in each region. Homogeneity of the CI was increased for all the subjects compared to T1wx2 (corresponding to uncorrected $P = 0.004$) except in the hippocampus. Discriminability of the CI was increased in the thalamus proper, the caudate, the putamen, and the pallidum compared to the T1wx2 image for all the subjects. For the hippocampus, one subject showed decreased discriminability in the CI. For the amygdala, seven of the nine subjects showed decreased discriminability in the CI compared to the T1wx2. For the accumbens area, three subjects showed decreased discriminability in CI compared to the T1wx2 image.

For the HCP data (Figure 5 and Table 2b), the main effect of image type was significant in homogeneity and discriminability. Tukey's multiple comparison test between image types indicated that both the homogeneity ($P = 0.001$) and the discriminability ($P < 0.001$) of the CI was significantly higher than the T1w image on average across the regions. A significant effect of region and an interaction between image type and region were also seen in both homogeneity and discriminability.

Table 5 shows the results of Tukey's multiple comparison test between image types in each region. Homogeneity was significantly increased with the CI in the putamen, the amygdala, and the accumbens area, but was significantly decreased in the pallidum compared to the T1w image. Discriminability of the CI was significantly increased in the caudate, the pallidum, and the accumbens area, while significantly decreased in the thalamus-proper compared to the T1w image.

To summarize the results of subcortical regions, all assessed regions except the pallidum in the HCP data showed homogeneity improvement in the CI or no difference in homogeneity versus the T1w image. Regarding the discriminability, the caudate, the putamen, the pallidum, the hippocampus, and the accumbens area showed either improved discriminability in the CI or no difference in discriminability from the T1w image. The thalamus-proper in the HCP data showed a significant decrease of discriminability in the CI compared to the T1w image. The amygdala showed decreased discriminability in the CI compared to T1w and T1wx2 images.

Discussion

We have introduced a novel approach for combining T1- and T2-weighted MR images to enhance homogeneity and discriminability between white matter and gray matter and between subcortical nuclei. The combined image significantly enhanced homogeneity within white matter and gray matter and also improved discriminability between the tissues. The CI also showed better discriminability compared to the average of two T1w images (T1wx2), which suggests that the combination of information from different modalities in the CI had more benefit than simply averaging images of the same modality.

Interestingly, the average of two T1w images did not improve the homogeneity and the discriminability compared to the single T1w image. This could be due to the fact that enhancing signal to noise ratio (SNR) by averaging does not necessarily enhance the signal homogeneity within a tissue. If SNR is high enough with a single image and bias field is a

major source of inhomogeneity, averaging two images would not substantially help to improve homogeneity.

This combination also enhanced the homogeneity and the discriminability of many subcortical structures although the effects differed somewhat between datasets and brain regions. The more modest improvement in homogeneity in the HCP data could be due to the fact that the preprocessed T1w images in the HCP data already had high homogeneity. However, homogeneity improvements were still seen in some regions, which indicate that CI can remove image inhomogeneity more aggressively than bias field correction.

For the amygdala region, discriminability was decreased in many subjects although the difference was not statistically significant. This result could suggest that the T1w-sT2w contrast of the amygdala was not distinguishable from adjacent regions more than that observed for the T1w image. For the thalamus-proper region, a reduction of discriminability was observed for the HCP data but discriminability was significantly improved in the LIBR dataset. Although the reason for the opposite results obtained in the LIBR and the HCP datasets in the thalamus-proper is unclear, the difference of scanning parameters might be relevant. HCP used longer TE for T2w to enhance the contrast for myelin detection (23,25). The increase of myelin contrast could reduce the homogeneity within a region and the discriminability between regions.

There are also other approaches using images to segment tissues with multivariate classification analysis (18-20,38,39). The difference between these approaches and the image fusion approach we took is that the former aims to create a discrete segmentation image while the later aims to improve the quality of the original image. While the multivariate classification approach could have better segmentation performance, creating a single fusion image still has a benefit in manual image inspection by human raters. Even though automatic segmentation is a major trend in recent structural analysis, manual segmentation analysis still has importance especially in delineating small structures like the habenula (40).

Approach of combining T1w and T2w images by dividing T1w by T2w (T1w/T2w) images was also recently proposed by Glasser and Van Essen (25) to provide a myelin content contrast. One should note, however, that the CI and T1w/T2w are different combined images with very different aims. The current approach aims to enhance homogeneity within a tissue and discriminability between tissues, whereas the T1w/T2w aims to enhance the contrast for myelin detection, so higher contrast within a tissue (lower homogeneity) in T1w/T2w is a desirable property for its purpose. The CI and T1w/T2w combinations serve different purposes.

Although the CI can be created with a simple equation, calculating a scaling factor after segmenting tissues could be a complex part of the process. This segmentation however does not need to be exact since only the median value of tissue is necessary to calculate the scaling factor. We used a tissue probability map on the template brain and no bias correction was done when calculating the scaling factor. This approach was sufficient as long we can assume that T1w and T2w images have similar bias field. Rather than a nonlinear warping

of template brain, a faster segmentation application (e.g. 3dSeg command in AFNI) could be used for estimating the median value of each tissue.

The advantage of combining multiple contrasts could be enhanced further by optimizing the imaging parameters. While the improvement with the CI was demonstrated by employing different imaging parameters, it does not mean that the CI is insensitive to scanning parameters. For example, TE of the T2w image had significant effects on the homogeneity of subcortical regions (Table 2a), so this scanning parameter is still one of the most important factors to enhance the image contrast. TE of T2w image could also be critical for inhomogeneity correction in the CI since the normalization factor in the CI removes only the inhomogeneity of receiving coil sensitivity (B1-) but does not remove transmit field inhomogeneity (B1+), which might affect differently the T1w and the T2w images. Further optimization of the TE in the T2w image can also potentially improve the contrast of iron-rich subcortical structures. We would like to stress that the CI is not an alternative to better or optimized T1w and T2w imaging sequences (2,41-44). Instead this simple approach can utilize improved T1w and T2w images and, by employing the CI combination, can further increase imaging contrast.

Conclusion

The CI approach remove image inhomogeneity without explicit bias field estimation and significantly improve discriminability between white matter and gray matter and many subcortical structures, with the exception of the amygdala and the thalamus. The quality enhancement offered by the CI can improve neuromorphometric analyses of the human brain.

Supplementary Material

Refer to Web version on PubMed Central for supplementary material.

Acknowledgement

This research was supported by the Laureate Institute for Brain Research and the William K. Warren Foundation and in part by R01MH098099 NIMH/NIH research grant. Wayne Drevets, M.D. is an employee of Johnson & Johnson, Inc., and has consulted for Myriad/Rules Based Medicine and Eisai, Inc. Jonathan Savitz, Ph.D. has received research funding from Janssen Pharmaceuticals for an independent study. Data were provided in part by the Human Connectome Project, WU-Minn Consortium (Principal Investigators: David Van Essen and Kamil Ugurbil; 1U54MH091657) funded by the 16 NIH Institutes and Centers that support the NIH Blueprint for Neuroscience Research; and by the McDonnell Center for Systems Neuroscience at Washington University.

References

1. Runge V. Current technological advances in magnetic resonance with critical impact for clinical diagnosis and therapy. Investigative radiology. 2013; 48(12):869–877. [PubMed: 24126386]
2. Marques JP, Kober T, Krueger G, van der Zwaag W, Van de Moortele PF, Gruetter R. MP2RAGE, a self bias-field corrected sequence for improved segmentation and T1-mapping at high field. Neuroimage. 2010; 49(2):1271–1281. [PubMed: 19819338]
3. Wansapura JP, Holland SK, Dunn RS, Ball WS Jr. NMR relaxation times in the human brain at 3.0 tesla. J Magn Reson Imaging. 1999; 9(4):531–538. [PubMed: 10232510]
4. Lu H, Nagae-Poetscher LM, Golay X, Lin D, Pomper M, van Zijl PC. Routine clinical brain MRI sequences for use at 3.0 Tesla. J Magn Reson Imaging. 2005; 22(1):13–22. [PubMed: 15971174]

5. Gelman N, Ewing JR, Gorell JM, Spickler EM, Solomon EG. Interregional variation of longitudinal relaxation rates in human brain at 3.0 T: relation to estimated iron and water contents. Magn Reson Med. 2001; 45(1):71–79. [PubMed: 11146488]

6. Wu Y, Warfield SK, Tan IL, Wells Iii WM, Meier DS, van Schijndel RA, Barkhof F, Guttmann CRG. Automated segmentation of multiple sclerosis lesion subtypes with multichannel MRI. Neuroimage. 2006; 32(3):1205–1215. [PubMed: 16797188]

7. Neema M, Stankiewicz J, Arora A, Dandamudi VS, Batt CE, Guss ZD, Al-Sabbagh A, Bakshi R. T1- and T2-based MRI measures of diffuse gray matter and white matter damage in patients with multiple sclerosis. Journal of neuroimaging : official journal of the American Society of Neuroimaging. 2007; 17(Suppl 1):16S–21S. [PubMed: 17425729]

8. Klawiter EC. Current and new directions in MRI in multiple sclerosis. Continuum (Minneapolis, Minn). 2013; 19(4):1058–1073. Multiple Sclerosis.

9. Datta S, Narayana PA. A comprehensive approach to the segmentation of multichannel three-dimensional MR brain images in multiple sclerosis. NeuroImage: Clinical. 2013; 2(0):184–196. [PubMed: 24179773]

10. de Bazelaire C, Rofsky NM, Duhamel G, Zhang J, Michaelson MD, George D, Alsop DC. Combined T2* and T1 measurements for improved perfusion and permeability studies in high field using dynamic contrast enhancement. European Radiology. 2006; 16(9):2083–2091. [PubMed: 16583215]

11. Min BD, Kim WT, Cho BS, Kim YJ, Yun SJ, Lee SC, Kim WJ. Usefulness of a combined approach of T1-weighted, T2-weighted, dynamic contrast-enhanced, and diffusion-weighted imaging in prostate cancer. Korean Journal of Urology. 2012; 53(12):830–835. [PubMed: 23301126]

12. Aydn H, Kzlgöz V, Tatar IG, Damar C, Ugan AR, Paker I, Hekimoglu B. Detection of prostate cancer with magnetic resonance imaging: Optimization of T1-weighted, T2-weighted, dynamic-enhanced T1-weighted, diffusion-weighted imaging apparent diffusion coefficient mapping sequences and MR spectroscopy, correlated with biopsy and histopathological findings. Journal of Computer Assisted Tomography. 2012; 36(1):30–45. [PubMed: 22261768]

13. Jara H, Sakai O, Mankal P, Irving RP, Norbash AM. Multispectral quantitative magnetic resonance imaging of brain iron stores: a theoretical perspective. Topics in magnetic resonance imaging : TMRI. 2006; 17(1):19–30. [PubMed: 17179894]

14. Maillard P, Delcroix N, Crivello F, Dufouil C, Gicquel S, Joliot M, Tzourio-Mazoyer N, Alperovitch A, Tzourio C, Mazoyer B. An automated procedure for the assessment of white matter hyperintensities by multispectral (T1, T2, PD) MRI and an evaluation of its between-centre reproducibility based on two large community databases. Neuroradiology. 2008; 50(1):31–42. [PubMed: 17938898]

15. Baudrexel S, Nürnberger L, Rüb U, Seifried C, Klein JC, Deller T, Steinmetz H, Deichmann R, Hilker R. Quantitative mapping of T1 and T2 discloses nigral and brainstem pathology in early Parkinson's disease. Neuroimage. 2010; 51(2):512–520. [PubMed: 20211271]

16. House PM, Lanz M, Holst B, Martens T, Stodieck S, Huppertz HJ. Comparison of morphometric analysis based on T1- and T2-weighted MRI data for visualization of focal cortical dysplasia. Epilepsy Research. 2013

17. Bhooshan N, Giger M, Lan L, Li H, Marquez A, Shimauchi A, Newstead GM. Combined use of T2-weighted MRI and T1-weighted dynamic contrast-enhanced MRI in the automated analysis of breast lesions. Magnetic Resonance in Medicine. 2011; 66(2):555–563. [PubMed: 21523818]

18. Alfano B, Brunetti A, Covelli EM, Quarantelli M, Panico MR, Ciarmiello A, Salvatore M. Unsupervised, automated segmentation of the normal brain using a multispectral relaxometric magnetic resonance approach. Magn Reson Med. 1997; 37(1):84–93. [PubMed: 8978636]

19. Lin GC, Wang CM, Wang WJ, Sun SY. Automated classification of multispectral MR images using unsupervised constrained energy minimization based on fuzzy logic. Magn Reson Imaging. 2010; 28(5):721–738. [PubMed: 20418040]

20. Murino L, Granata D, Carfora MF, Selvan SE, Alfano B, Amato U, Larobina M. Evaluation of supervised methods for the classification of major tissues and subcortical structures in multispectral brain magnetic resonance images. Computerized medical imaging and graphics : the

official journal of the Computerized Medical Imaging Society. 2014; 38(5):337–347. [PubMed: 24702776]

21. Van de Moortele PF, Auerbach EJ, Olman C, Yacoub E, Ugurbil K, Moeller S. T1 weighted brain images at 7 Tesla unbiased for Proton Density, T2* contrast and RF coil receive B1 sensitivity with simultaneous vessel visualization. Neuroimage. 2009; 46(2):432–446. [PubMed: 19233292]
22. Helms G, Kallenberg K, Dechent P. Contrast-driven approach to intracranial segmentation using a combination of T2- and T1-weighted 3D MRI data sets. Journal of Magnetic Resonance Imaging. 2006; 24(4):790–795. [PubMed: 16929528]
23. Glasser MF, Sotiropoulos SN, Wilson JA, Coalson TS, Fischl B, Andersson JL, Xu J, Jbabdi S, Webster M, Polimeni JR, Van Essen, Jenkinson M, Consortium WU-MH. The minimal preprocessing pipelines for the Human Connectome Project. Neuroimage. 2013; 80:105–124. [PubMed: 23668970]
24. Rilling JK, Glasser MF, Jbabdi S, Andersson J, Preuss TM. Continuity, divergence, and the evolution of brain language pathways. Frontiers in evolutionary neuroscience. 2011; 3:11. [PubMed: 22319495]
25. Glasser MF, Van Essen DC. Mapping human cortical areas in vivo based on myelin content as revealed by T1- and T2-weighted MRI. J Neurosci. 2011; 31(32):11597–11616. [PubMed: 21832190]
26. Van Essen DC, Smith SM, Barch DM, Behrens TE, Yacoub E, Ugurbil K, Consortium WU-MH. The WU-Minn Human Connectome Project: An overview. Neuroimage. 2013; 80:62–79. [PubMed: 23684880]
27. Haacke, EM.; Brown, R.; Thompson, M.; Venkatesan, R. John Wiley and Sons; New York: 1999. Magnetic resonance imaging: physical principles and sequence design.
28. Savitz JB, Rauch SL, Drevets WC. Reproduced from Habenula volume in bipolar disorder and major depressive disorder: a high-resolution magnetic resonance imaging study. Mol Psychiatry. 2013; 18(5):523. [PubMed: 23608961]
29. Misaki, M.; Victor, T.; Suzuki, H.; Teague, K.; McKinney, B.; Bellgowan, P.; Savitz, J.; Drevets, W.; Bodurka, J. Subtypes of nucleus accumbens activations for anticipation of gains and losses in healthy and depressed subjects; Joint Annual meeting ISMRM-ESMRMB; Milan, Italy. 2014. p. 0832
30. Cox RW. AFNI: software for analysis and visualization of functional magnetic resonance neuroimages. Comput Biomed Res. 1996; 29(3):162–173. [PubMed: 8812068]
31. Ugurbil K, Xu J, Auerbach EJ, Moeller S, Vu AT, Duarte-Carvajalino JM, Lenglet C, Wu X, Schmitter S, Van de Moortele PF, Strupp J, Sapiro G, De Martino F, Wang D, Harel N, Garwood M, Chen L, Feinberg DA, Smith SM, Miller KL, Sotiropoulos SN, Jbabdi S, Andersson JL, Behrens TE, Glasser MF, Van Essen DC, Yacoub E, Consortium WU-MH. Pushing spatial and temporal resolution for functional and diffusion MRI in the Human Connectome Project. Neuroimage. 2013; 80:80–104. [PubMed: 23702417]
32. Fonov V, Evans AC, Botteron K, Almli CR, McKinstry RC, Collins DL. Unbiased average age-appropriate atlases for pediatric studies. Neuroimage. 2011; 54(1):313–327. [PubMed: 20656036]
33. Avants BB, Epstein CL, Grossman M, Gee JC. Symmetric diffeomorphic image registration with cross-correlation: evaluating automated labeling of elderly and neurodegenerative brain. Med Image Anal. 2008; 12(1):26–41. [PubMed: 17659998]
34. Tustison NJ, Avants BB, Cook PA, Zheng Y, Egan A, Yushkevich PA, Gee JC. N4ITK: improved N3 bias correction. IEEE Trans Med Imaging. 2010; 29(6):1310–1320. [PubMed: 20378467]
35. Duda, RO.; Hart, P.; Stork, DG. Pattern Classification. John Wiley and Sons; New York: 2000.
36. Pinheiro J, Bates D. Mixed Effects Models in S and S-Plus: Springer. 2000
37. R Core Team. R: A Language and Environment for Statistical Computing. R Foundation for Statistical Computing; Vienna, Austria: URL http://www.R-project.org/;2014/7/10
38. Harris G, Andreasen NC, Cizadlo T, Bailey JM, Bockholt HJ, Magnotta VA, Arndt S. Improving tissue classification in MRI: a three-dimensional multispectral discriminant analysis method with automated training class selection. J Comput Assist Tomogr. 1999; 23(1):144–154. [PubMed: 10050826]

39. Aubert-Broche B, Grova C, Pike GB, Collins DL. Clustering of atlas-defined cortical regions based on relaxation times and proton density. Neuroimage. 2009; 47(2):523–532. [PubMed: 19426811]

40. Savitz JB, Nugent AC, Bogers W, Roiser JP, Bain EE, Neumeister A, Zarate CA Jr. Manji HK, Cannon DM, Marrett S, Henn F, Charney DS, Drevets WC. Habenula volume in bipolar disorder and major depressive disorder: a high-resolution magnetic resonance imaging study. Biol Psychiatry. 2011; 69(4):336–343. [PubMed: 21094939]

41. Sudhyadhom A, Haq IU, Foote KD, Okun MS, Bova FJ. A high resolution and high contrast MRI for differentiation of subcortical structures for DBS targeting: the Fast Gray Matter Acquisition T1 Inversion Recovery (FGATIR). Neuroimage. 2009; 47(Suppl 2):T44–52. [PubMed: 19362595]

42. Tanner M, Gambarota G, Kober T, Krueger G, Erritzoe D, Marques JP, Newbould R. Fluid and white matter suppression with the MP2RAGE sequence. J Magn Reson Imaging. 2012; 35(5): 1063–1070. [PubMed: 22170818]

43. Marques JP, Gruetter R. New developments and applications of the MP2RAGE sequence--focusing the contrast and high spatial resolution R1 mapping. PLoS One. 2013; 8(7):e69294. [PubMed: 23874936]

44. Tourdias T, Saranathan M, Levesque IR, Su J, Rutt BK. Visualization of intra-thalamic nuclei with optimized white-matter-nulled MPRAGE at 7T. Neuroimage. 2014; 84:534–545. [PubMed: 24018302]

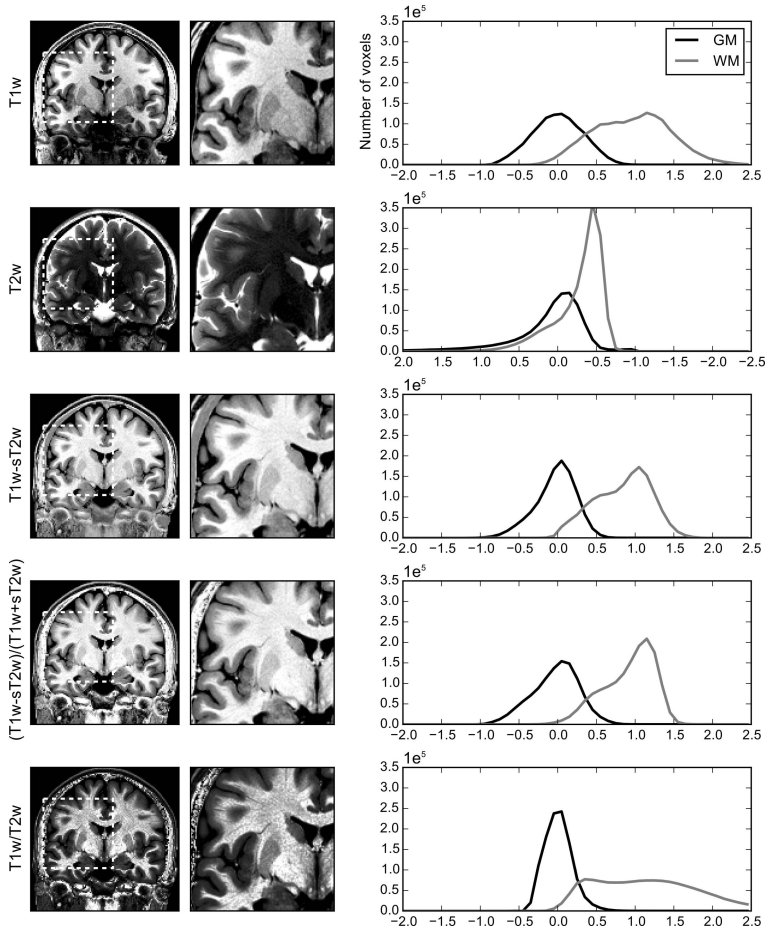

Figure 1.

One coronal slice of T1w, T2w, T1w-sT2w, CI ((T1w-sT2w)/(T1w+sT2w)), and T1w/T2w images for one representative subject (left column). The right images are zoomed regions of the left images marked with the white dotted square. For each image contrast, brain voxels within 5% to 95% of signal intensity distribution were mapped onto the display scale (0-255). The right column shows distribution plots of normalized intensity values for gray matter (GM) and white matter (WM) voxels from the whole brain. Voxels within 5% to 95% of signal intensity distribution for the whole brain were mapped onto −1.5 to 1.5 range with centering the median of GM voxels to be zero. The direction of horizontal axis of T2w distribution plot was reversed for comparing with other image types.

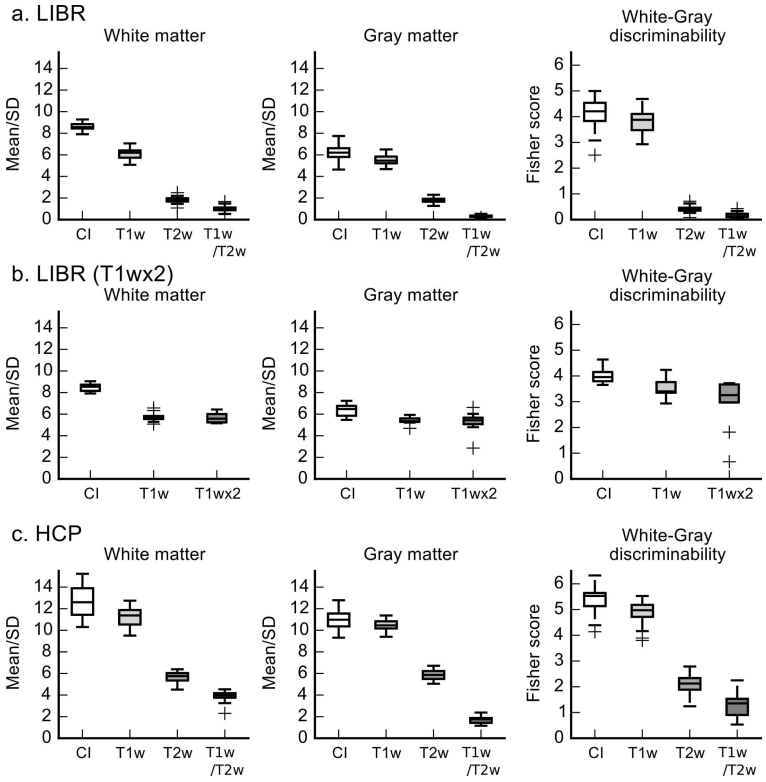

Figure 2.

Box plots of homogeneity (mean/SD) and discriminability (Fisher score, FS) of white and gray matter for the CI, T1w, T2w, and T1w/T2w of the LIBR data (a), LIBR data for T1wx2, and HCP data (c). The box indicates the range between the first and third quartiles, and the horizontal line in the box is the median. The vertical lines from the box indicate the range of all values within the 1.5 × interquartile range (IQR) from the edge of the box. Plus signs show the samples out of 1.5 × IQR.

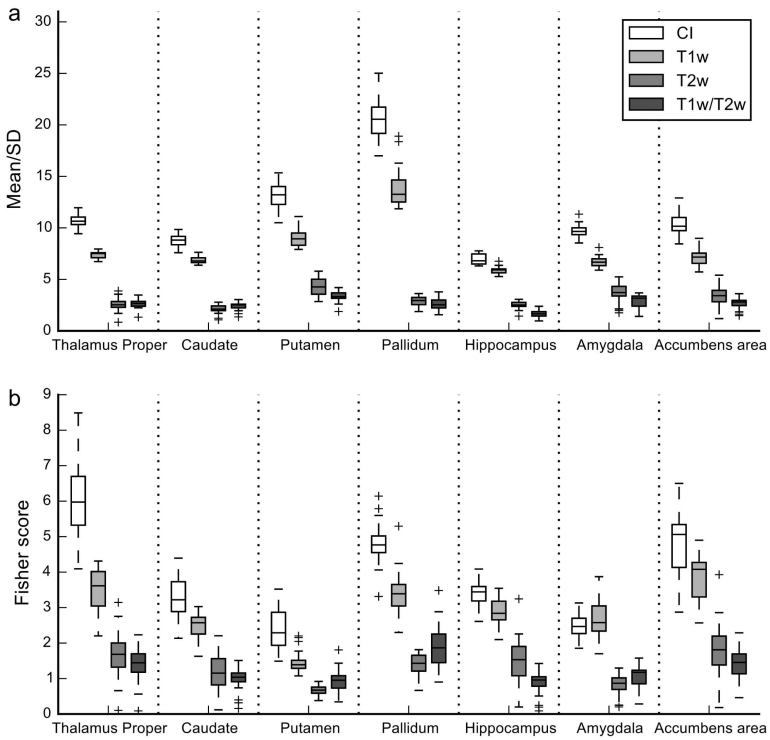

Figure 3.

Box plots of homogeneity (mean/SD) and discriminability (Fisher score) of subcortical regions for the CI, T1w, T2w, and T1w/T2w of the LIBR data. Conventions are the same as in Figure 2.

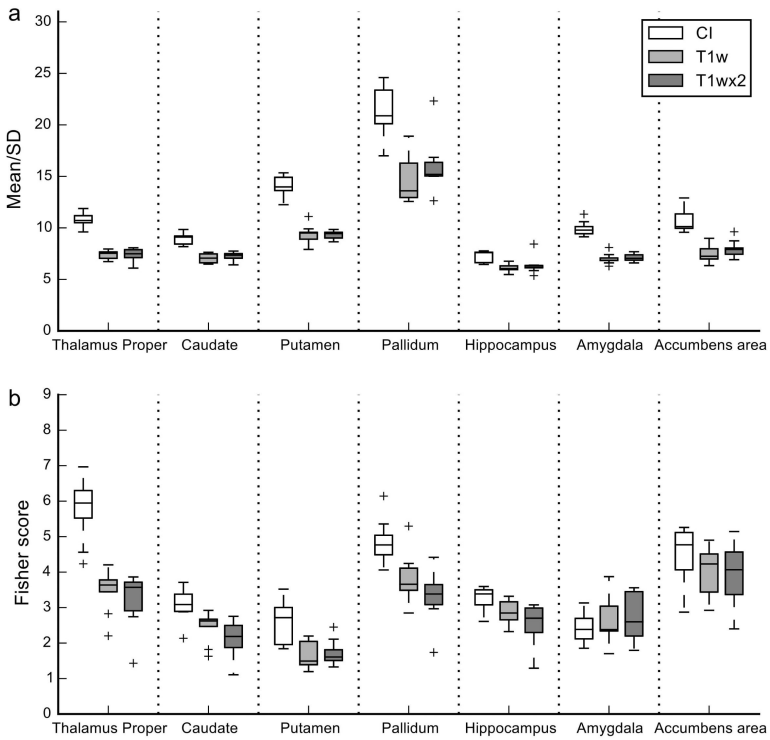

Figure 4.

Box plots of homogeneity (mean/SD) and discriminability (Fisher score) of subcortical regions for the CI, T1wx2, and T1w of the LIBR data. Conventions are the same as in Figure 2.

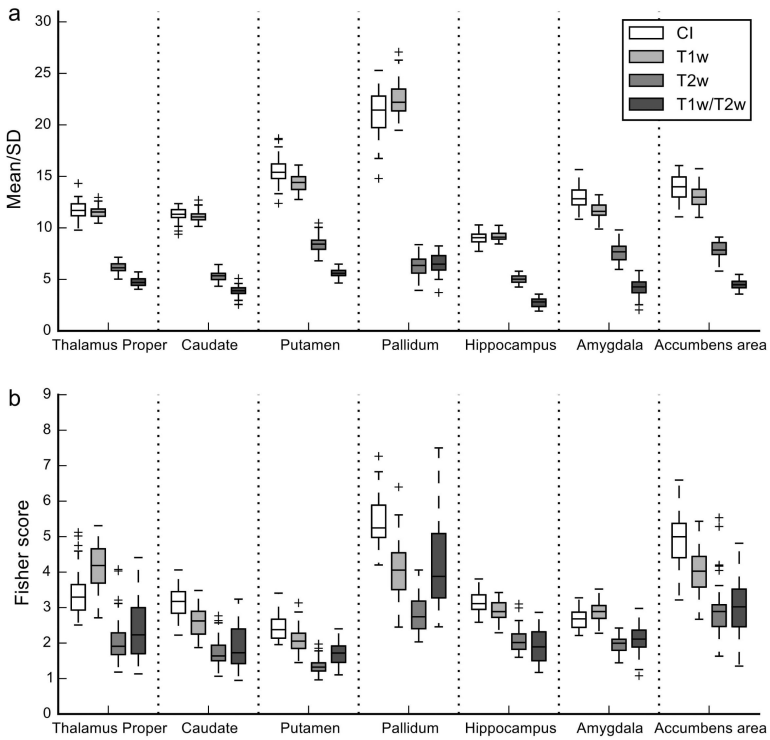

Figure 5.

Box plots of homogeneity (mean/SD) and discriminability (Fisher score) of subcortical regions for the CI, T1w, T2w, and T1w/T2w of the HCP data. Conventions are the same as in Figure 2.

Table 1

Statistics of the linear mixed effect model analysis for white matter homogeneity, gray matter homogeneity, and white-gray discriminability in the LIBR (a) and HCP (b) dataset.

		White matter homogeneity		Gray matter homogeneity		White-Gray discriminability	
	df	***F***	***P***	***F***	***P***	***F***	***P***
a. LIBR							
Image type	3, 66	2717.608	< .001***	1473.21	< .001***	850.805	< .001***
Age	1, 17	7.775	.013*	0.875	.363	0.046	.832
Sex	1, 17	3.485	.079	2.249	.152	2.233	.153
T2 TR	1, 17	0.063	.806	1.887	.187	0.751	.398
T2 TE	1, 17	6.619	.020*	2.740	.116	0.200	.661
T2 FA	1, 17	0.004	.950	0.294	.595	0.464	.505
b. HCP							
Image type	3,111	1751.473	< .001***	2795.204	< .001***	1867.607	< .001***
Sex	1, 36	0.165	.687	0.301	.587	5.246	.028

Table 2

Statistics of the linear mixed effect model analysis for homogeneity and discriminability of subcortical regions in the LIBR (a) and HCP (b) dataset.

		Homogeneity		Discriminability	
	df	***F***	***P***	***F***	***P***
a. LIBR					
Image type	3, 594	3733.249	< .001***	1167.278	< .001***
Region	6, 594	412.709	< .001***	181.565	< .001***
Age	1, 17	0.000	.987	2.810	.112
Sex	1, 17	15.366	.001**	0.049	.827
T2 TR	1, 17	0.316	.581	0.001	.971
T2 TE	1, 17	14.881	.001**	0.888	.359
T2 FA	1, 17	3.004	.101	1.886	.188
Image type x Region	12, 440	131.504	< .001***	30.741	< .001***
b. HCP					
Image type	3, 999	6190.254	< .001***	520.697	< .001***
Region	6, 999	891.064	< .001***	434.316	< .001***
Sex	1, 36	0.326	.571	0.149	.701
Image type x Region	18, 999	165.345	< .001***	24.806	< .001***

Table 3

The z values of Tukey's multiple comparison for homogeneity (Homo) and discriminability (Disc) between CI, T1w, T2w, and T1w/T2w of the LIBR dataset in subcortical regions.

	CI – T1w		CI – T2w		CI – T1w/T2w	
Region	**Homo**	**Disc**	**Homo**	**Disc**	**Homo**	**Disc**
Thalamus proper	12.101***	17.518***	31.919***	30.454***	31.576***	32.389***
Caudate	7.691***	5.674***	26.946***	14.710***	25.366***	16.119***
Putamen	16.816***	6.474***	34.068***	12.173***	37.907***	10.187***
Pallidum	26.023***	9.834***	67.395***	24.175***	68.638***	20.435***
Hippocampus	3.796**	3.828**	16.545***	13.480***	19.840***	17.702***
Amygdala	12.808***	−1.145	23.563***	11.798***	26.945***	10.053***
Accumbens area	11.710***	6.990***	25.606***	21.534***	29.168***	24.143***

**: $P<0.01$,

***: $P < 0.001$

Table 4

The *P* values of Wilcoxon signed rank test for the homogeneity and discriminability between CI, T1wx2, and T1w of the LIBR data in subcortical regions. The value in the parenthesis after *P* value indicates the number of subjects who had decreased homogeneity or discriminability in the CI compared to T1wx2 or T1w.

	CI – T1w		CI – T1wx2	
Region	**Homogeneity**	**Discriminability**	**Homogeneity**	**Discriminability**
Thalamus proper	.004 (0)	.004 (0)	.004 (0)	.004 (0)
Caudate	.004 (0)	.004 (0)	.004 (0)	.004 (0)
Putamen	.004 (0)	.004 (0)	.004 (0)	.004 (0)
Pallidum	.004 (0)	.004 (0)	.004 (0)	.004 (0)
Hippocampus	.004 (0)	.027 (1)	.027 (1)	.020 (1)
Amygdala	.004 (0)	.359 (6)	.004 (0)	.496 (7)
Accumbens area	.004 (0)	.012 (2)	.004 (0)	.098 (3)

Table 5

The z values of Tukey's multiple comparison test for intensity homogeneity (Homo) and discriminability (Disc) between CI, T1w, T2w, and T1w/T2w of the HCP dataset in subcortical regions.

	CI – T1w		CI – T2w		CI – T1w/T2w	
Region	**Homo**	**Disc**	**Homo**	**Disc**	**Homo**	**Disc**
Thalamus proper	0.527	−6.322***	23.879***	12.210***	30.949***	9.489***
Caudate	1.298	4.805***	27.077***	12.607***	33.864***	11.519***
Putamen	5.517***	3.182	33.482***	10.079***	45.686***	6.878***
Pallidum	−8.153***	11.211***	64.478***	23.292***	63.038***	9.994***
Hippocampus	−0.174	2.167	18.663***	9.583***	29.099***	11.104***
Amygdala	6.024***	−1.706	24.831***	6.557***	40.225***	5.266
Accumbens area	3.679**	8.934***	29.990***	18.085***	44.782***	16.947***

** : $P < 0.01$,

*** : $P < 0.001$